Computers in Biology and Medicine 176 (2024) 108555

Contents lists available at ScienceDirect

Computers in Biology and Medicine

journal homepage: www.elsevier.com/locate/compbiomed

ECG waveform generation from radar signals: A deep learning perspective

Farhana Ahmed Chowdhury [a], Md Kamal Hosain [a], Md Sakib Bin Islam [b], Md Shafayet Hossain [c], Promit Basak [d], Sakib Mahmud [e], M. Murugappan [f,g,*], Muhammad E.H. Chowdhury [e,**]

[a] Department of Electronics and Telecommunication Engineering, Rajshahi University of Engineering and Technology, Rajshahi, 6204, Bangladesh
[b] Department of Biomedical Engineering, Military Institute of Science and Technology, Dhaka, Bangladesh
[c] Department of Electrical, Electronics and Systems Engineering, Universiti Kebangsaan Malaysia, Bangi, Selangor, 43600, Malaysia
[d] Department of Electrical and Electronic Engineering, University of Dhaka, Dhaka, 1000, Bangladesh
[e] Department of Electrical Engineering, Qatar University, Doha, 2713, Qatar
[f] Intelligent Signal Processing (ISP) Research Lab, Department of Electronics and Communication Engineering, Kuwait College of Science and Technology, Block 4, Doha, Kuwait
[g] Department of Electronics and Communication Engineering, Vels Institute of Sciences, Technology, and Advanced Studies, Chennai, Tamilnadu, India

ARTICLE INFO

Keywords:
ECG
Raw radar data
MultiResLinkNet
CNN
Deep learning

ABSTRACT

Cardiovascular diagnostics relies heavily on the ECG (ECG), which reveals significant information about heart rhythm and function. Despite their significance, traditional ECG measures employing electrodes have limitations. As a result of extended electrode attachments, patients may experience skin irritation or pain, and motion artifacts may interfere with signal accuracy. Additionally, ECG monitoring usually requires highly trained professionals and specialized equipment, which increases the treatment's complexity and cost. In critical care scenarios, such as continuous monitoring of hospitalized patients, wearable sensors for collecting ECG data may be difficult to use. Although there are issues with ECG, it remains a valuable tool for diagnosing and monitoring cardiac disorders due to its non-invasive nature and the detailed information it provides about the heart. The goal of this study is to present an innovative method for generating continuous ECG waveforms from non-contact radar data by using Deep Learning. The method can eliminate the need for invasive or wearable biosensors and expensive equipment to collect ECGs. In this paper, we propose the MultiResLinkNet, a one-dimensional convolutional neural network (1D CNN) model for generating ECG signals from radar waveforms. With the help of a publicly accessible radar benchmark dataset, an end-to-end DL architecture is trained and assessed. There are six ports of raw radar data in this dataset, along with ground truth physiological signals collected from 30 participants in five distinct scenarios: Resting, Valsalva, Apnea, Tilt-up, and Tilt-down. By using strong temporal and spectral measurements, we assessed our proposed framework's ability to convert ECG data from Radar signals in three distinct scenarios, namely Resting, Valsalva, and Apnea (RVA). ECG segmentation performed better by MultiResLinkNet than by state-of-the-art networks in both combined and individual cases. As a result of the simulations, the resting, valsalva, and RVA scenarios showed the highest average temporal values, respectively: 66.09523 ± 19.33, 60.13625 ± 21.92, and 61.86265 ± 21.37. In addition, it exhibited the highest spectral correlation values (82.4388 ± 18.42 (Resting), 77.05186 ± 23.26 (Valsalva), 74.65785 ± 23.17 (Apnea), and 79.96201 ± 20.82 (RVA)), along with minimal temporal and spectral errors in almost every case. The qualitative evaluation revealed strong similarities between generated and actual ECG waveforms. As a result of our method of forecasting ECG patterns from remote radar data, we can monitor high-risk patients, especially those undergoing surgery.

* Corresponding author. Intelligent Signal Processing (ISP) Research Lab, Department of Electronics and Communication Engineering, Kuwait College of Science and Technology, Block 4, Doha, Kuwait.
** Corresponding author.
E-mail addresses: m.murugappan@kcst.edu.kw (M. Murugappan), mchowdhury@qu.edu.qa (M.E.H. Chowdhury).

https://doi.org/10.1016/j.compbiomed.2024.108555
Received 19 April 2024; Received in revised form 1 May 2024; Accepted 5 May 2024
Available online 11 May 2024

1. Introduction and related works

Heartbeat monitoring plays a crucial role in monitoring human health and in detecting various heart disorders. Electrocardiogram (ECG) signals, which records the heart's electrical activity and displays its characteristics, such as the P-wave, the QRS complex, and the T-wave, it is commonly used to detect heartbeats [1,2]. An ECG signal, displayed in Fig. 1, offers significant knowledge about the activity of the heart, including the specific timing and appearance of P-waves, QRS complexes, and T-waves [3–5]. These characteristics are crucial for detecting different types of cardiac dysfunctions. Traditional techniques for continuous monitoring of ECG use wet electrodes, but developing non-contact technologies employ Doppler sensors to measure chest movement generated by the heartbeat. The majority of current techniques [6–8] rely on Doppler sensors to approximate heart rate or beat-to-beat intervals without accurately recording specific pulse characteristics such as P-waves, T-waves, and R-peaks. A variety of cardiac conditions, including arrhythmia, long QT syndrome, and aortic stenosis, can be diagnosed using these characteristics.

In addition to heartbeat detection [6,10,11], respiration rate detection [6,12], and activity identification [13], researchers have explored the use of the Doppler sensor in several other areas. Compared to breathing and minor body movements, cardiac components usually have a much lower Signal-to-Noise Ratio (SNR). As a result, various approaches for detecting the pulse with Doppler sensors have been proposed [6–16]. Heartbeats can be detected with high accuracy using these traditional techniques for calculating beat-to-beat intervals (BBIs) and heart rates (HRs). Even though analyzing the timings of these characteristics might help identify different cardiac conditions, the P-wave, T-wave, and R-peak have not been detected using traditional methods. The signal-to-noise ratio (SNR) of the heartbeat components can be reduced by breathing and minor body movements. Detecting the P-wave, T-wave, and R-peak poses a greater challenge than detecting the pulse alone.

Thus, several methodologies have been proposed for the processing of more complex signals [9,17–21]. Yamamoto et al. [9] provide a technique for reconstructing the ECG signal using a Doppler sensor to identify the P-wave, T-wave, and R-peak. As part of this approach, a hybrid DL model combining a Convolutional Neural Network (CNN) and a Long Short Term Memory (LSTM) is used. The researchers utilize DL to synthesize the ECG signal directly from raw radar data, eliminating the need for traditional ECG sensors. To automatically extract features and reconstruct the ECG signal, the proposed method utilizes a hybrid model that combines Convolutional Neural Networks (CNNs) and Long Short-Term Memory (LSTMs). Due to noise interference, the Doppler sensor's detection of the heartbeat signal may be distorted. Consequently, heartbeat signals display a variety of waveforms. While Petrovic et al. [18] addressed the problem from a distinct perspective. They presented a novel method that utilizes a 24-GHz Doppler radar to estimate heart rate variability (HRV) features. The program effectively measured beat-to-beat intervals (BBIs) and computed four HRV components by integrating frequency and temporal domain data. Testing conducted on actual data revealed mean relative errors ranging from 1.02 % to 2.07 % when compared to ECG readings. The radar-extracted HRV features showed strong agreement with the ECG-extracted HRV features, indicating that the radar system is well-suited for real-time monitoring.

A continuous wave Doppler radar system with a bandpass filter was used to extract the harmonic signal of heartbeats from chest surface vibrations. During the harmonic phase of the pulse, breathing is assumed to be absent. A gamma filter was used by Saluja et al. [17] to eliminate the harmonics associated with breathing through machine learning. Bodily movement is not considered in these techniques since they were developed to remove respiratory harmonics. In contrast to breathing, bodily motion occurs at a very wide amplitude and does not occur within a defined frequency range. Therefore, pre-informative methods such as frequency filters and gamma filters are not suitable for removing body motion. In contrast, a matched filter (MF) can be used to adjust itself depending on body movement. The function of a matched filter is to enhance the desired signal by converging it with the input signal, assuming the waveform's shape has already been determined. The approach is similar to correlation detection in receivers and template matching in machine learning. It is necessary to create a template of the heartbeat to extract heartbeats from chest vibrations using MF.

Based on "Preferred Reporting Items for Systematic Reviews and Meta-Analyses" (PRISMA) principles for scoping reviews, Nocera et al. [22] executed an investigation that explored the progress achieved by machine learning for detecting physiological signals. The study aimed to offer a detailed summary of the various machine learning and DL approaches used in analyzing RADAR recordings. They were primarily interested in investigating the most recent advances and uses in the regression of physiological signals and parameters. A wavelet transform (WT) was used by Bagwe et al. [23] to denoise radar signals. This stage removes noisy data using stages such as a power envelope, Hilbert Transform, and wavelet transform. In the second step, radar data is used to train an LSTM model to track radar signals. Based on radar emissions, Chen et al. [24] present a DL-based method for open-set person identification using radar emissions. The radar signals are preprocessed and separated into fixed-length samples before training. Signal samples are represented as points in the suggested feature space to distinguish

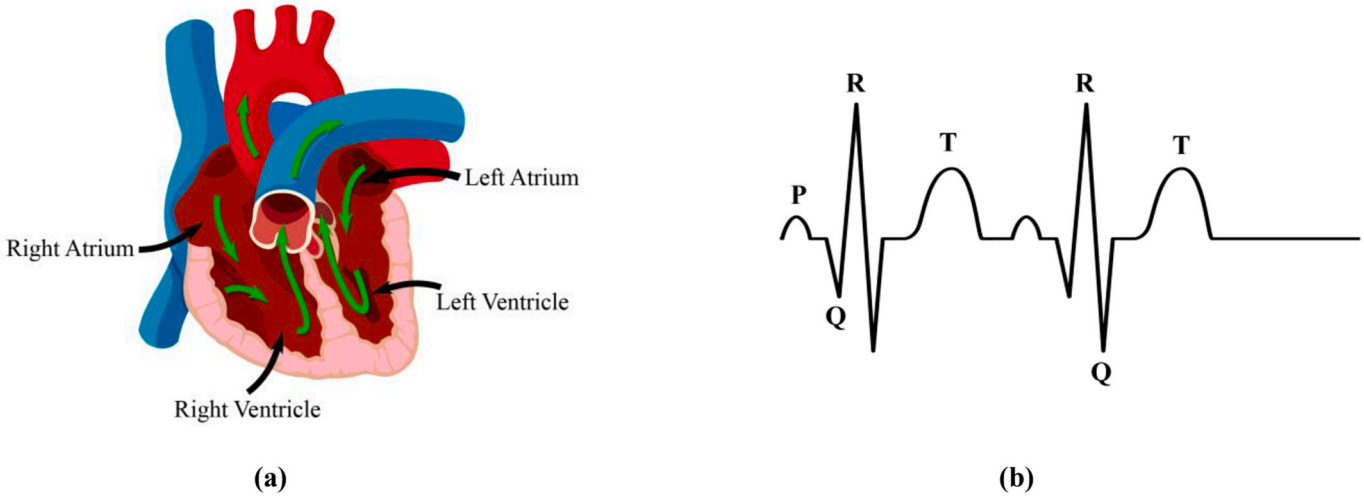

Fig. 1. Visualization of an illustrated heart and an ECG signal [9].

unknown from labeled signals. On the PTB-XL dataset, Smigiel et al. [25] classified ECG signals using Deep Neural Networks (DNNs). A neural network topology is used to classify ECG signals based on entropy-based characteristics and QRS complexes extracted from the signals. Xiang et al. [26] developed a "masked phase autoencoder with a vision transformer network" (MVN) for estimating heart rates from radar signals. Masked autoencoders (MAEs) are used for self-supervised pretraining, and a vision transformer (ViT) is used for transfer learning. During phase preprocessing, phase diffraction, and interpolation smoothing are performed on the input phase signal. A masked self-supervised training on the phase signal is done using the MAE network during pretraining. In their paper, Choi et al. [27] present various approaches that can be applied to radar-based people counting (RPC) tasks using DL. In the new preprocessing pipelines, raw radar echoes are translated into a better format for deep neural networks. Secondly, they create a new backbone architecture that reflects radar signals' spatiotemporal properties and reduces training load. In addressing the issue of ECG signal reconstruction, TODA et al. [28] created an innovative model capable of reconstructing the signal at a stationary state with the same level of accuracy as conventional methods. Their initial investigation was conducted in an environment characterized by low signal-to-noise ratio (SNR) and additive sine wave noise. Furthermore, Siuly et al. [29] introduced an innovative approach that employs a Time-Frequency Representation (TFR) based AlexNet CNN model for the diagnosis of Parkinson's disease (PD) using EEG data. By utilizing the Wavelet Scattering Transform (WST) to capture both temporal and spectral characteristics, and the AlexNet CNN to identify spatial patterns, the researchers achieved remarkable accuracies of 99.84 % and 95.79 % on the San Diego and Iowa datasets respectively. These results surpassed the performance of existing methods for detecting Parkinson's Disease (PD) based on electroencephalogram (EEG) data.

The effective application of DL in the annotation of protein functions, as demonstrated by AnnoPRO, demonstrates the capacity of sophisticated computational methods to tackle enduring obstacles in the biological sciences. AnnoPRO is an innovative strategy for protein function annotation proposed by Zheng et al. [30]. By combining a hybrid DL framework with a sequence-based multi-scale protein representation, AnnoPRO effectively tackles the long-tail challenge that is intrinsic to current approaches to function annotation. In addition, Mou et al. [31] provide EnsemPPIS, an innovative ensemble framework for forecasting protein-protein interaction (PPI) sites. EnsemPPIS combines transformer and gated convolutional networks to effectively capture both global and local patterns, as well as residue interactions. This approach achieves exceptional performance and has a wider range of applications compared to other current approaches. The interpretability of EnsemPPIS demonstrates its ability to learn residue interactions only from primary sequences, hence improving the accuracy of PPI site prediction. Expanding on these progressions, Wang et al. [32] provide a specialized encoding approach for RNAs and RNA-associated interactions. This unique technique successfully encodes a wide range of RNA features and allows for the integration of interacting partners in a task-specific manner using convolutional autoencoder-directed feature embedding. These results highlight the potential of DL approaches to completely transform our knowledge of biological processes, opening up new possibilities for creative applications in different physiological and pathological situations.

The main purpose of this present study is to establish a non-intrusive and remote method for monitoring ECG signals using radar data. This technique uses DL models for uninterrupted and extended ECG waveform monitoring, resulting in accurate waveform analysis. According to Schellenberger et al. [33], they published a dataset with radar vital signs synchronized with physiological waveforms such as ECG, ABP (Arterial Blood Pressure), and ICG (Impedance Cardiography). There are five distinct states of the patient in the dataset: resting, Valsalva, apnea, tilt-up, and tilt-down. DL-based 1D-segmentation models are used to synthesize/reconstruct ECG signals from radar data for the Resting, Valsalva, and Apnea scenarios. In this way, the ECG can be monitored continuously without causing any discomfort to the test subjects. We present the MultiResLinkNet model, a novel 1D CNN model that effectively generates normalized ECG signals from radar waveforms. In addition, we compared the results with three other popular 1D CNN models: Feature Pyramid Network (FPN) [34], UNet [35], and LinkNet [36].

As a result of this study, the following key contributions were made.

- This study thoroughly explores the use of non-contact, remote radar signals for producing ECG waveforms using DL-based 1D segmentation models.
- We have developed MultiResLinkNet, a reconstruction network that generates ECG segments from radar data. Performance comparisons of MultiResLinkNet and the current leading approaches have been conducted.
- In our method, raw radar data is used to produce ECG waveforms by exploiting only the in-phase (I) and quadrature (Q) components, thus eliminating the need for wearable sensors. Due to this feature, it is appropriate for extended surveillance of patients in both medical and domestic settings.
- A wide range of performance metrics are utilized to evaluate the proposed approach, guaranteeing its resilience and suitability in a variety of contexts.

Here is the structure of this paper: In Section 2, we present our method for synthesizing ECG signals from radar data. Moreover, this section provides a comprehensive description of MultiResLinkNet, a 1D segmentation model based on DL, and a summary of the benchmark dataset and the data preprocessing methods. In Section 3, the experimental configuration and evaluation measures used to evaluate the DL models are described. A comparison between our proposed segmentation network and three other cutting-edge segmentation networks is presented in Section 4. In Section 5, the limitations of this study are discussed with future directions, and in Section 6, the paper is concluded.

2. Methods and materials

This section discusses the process of synthesizing ECG from radar data. We begin by briefly outlining the framework's major elements before diving into its details. The next section provides an overview of the MultiResLinkNet signal reconstruction model used for ECG estimation. Next, we discuss the benchmark dataset and the data preparation techniques used in the study.

2.1. Overview of the framework: transformation of radar data to ECG data domain

We present a framework for estimating ECG patterns using radar signals based on several key components (Fig. 2), including the data preprocessing pipeline, 1D–CNN–based segmentation, and post-processing modules. As shown in Fig. 2(i), the system proposed in Ref. [37] can be seen in its overall layout.

During this study, data were acquired using a six-port interferometry technique, originally developed by Engen and Hoer in the 1970s to measure power. As outlined in Refs. [37,38], this technique was chosen for its efficiency in determining distance accurately. The radar system has six ports and operates at 24 GHz in the Industrial, Scientific, and Medical (ISM) band. This device incorporates a Wilkinson power divider and three quadrature hybrid couplers to guarantee phase accuracy. It is also cost-effective and energy-efficient. A transmitter and a receiver antenna are used in the RF front-end of the radar system (Fig. 2(i)) to transmit and receive, respectively, the transmitting and reflected waveforms of the subject being studied. A primary approach to

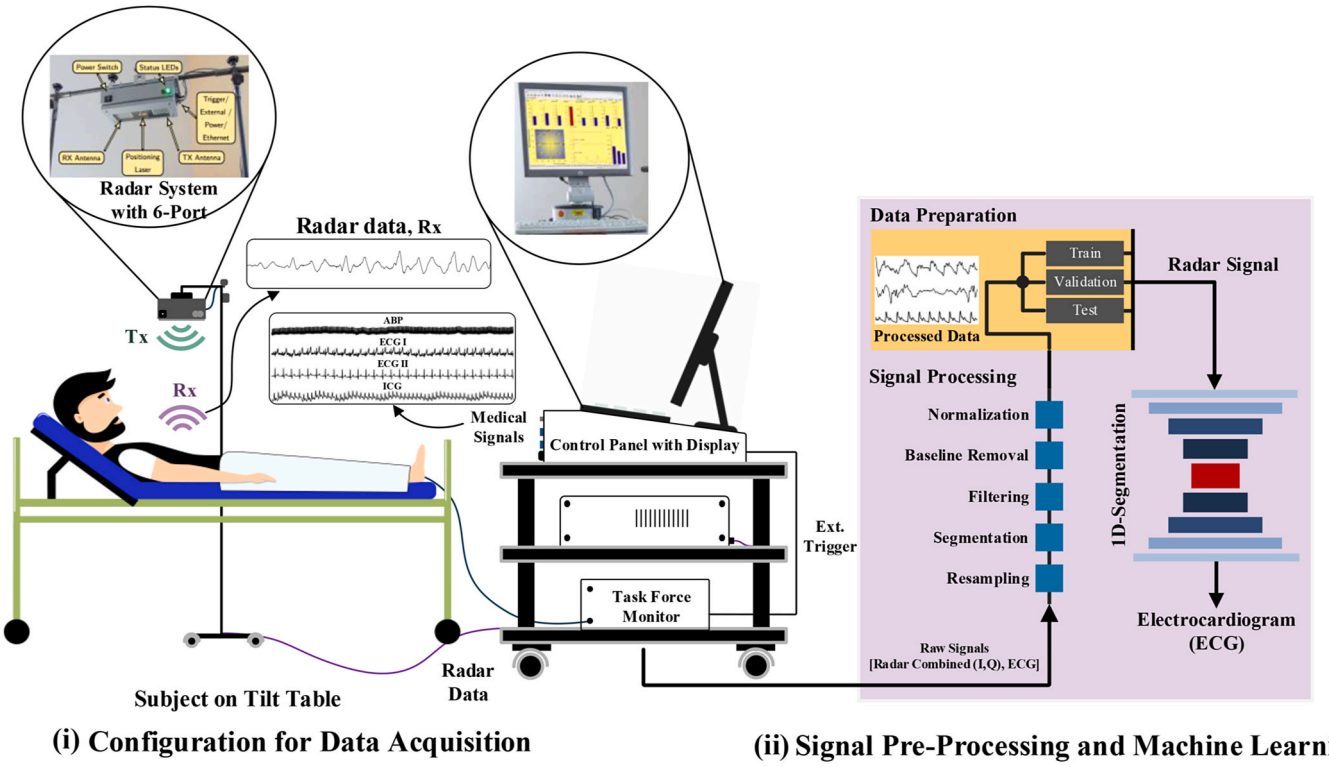

Fig. 2. Diagram illustrating the suggested framework for synthesizing ECG from radar waveforms. (i) The configuration for collecting data from the dataset provided by Schellenberger et al. [33]. (ii) The suggested framework for radar-based estimation of ECG patterns.

obtaining single-channel radar data from raw radar signal waveforms (In-phase (I) and Quadrature (Q) components) involves digitization, elliptical fitting, and arctangent modulation [37]. A phase signal can be used to determine the relative distance by following these steps. Using ellipse fitting, we can accurately determine the phase of the radar from raw data by reducing the interference between the transmitting (Tx) and receiving (Rx) antennas and minimizing the gain errors. Distance information is derived from a combination of physiological measurements, such as ECG [39], PCG [38], SCG [40], ABP [41], Resp [37], and others. Given the wavelength (λ) of the Tx, the change in displacement Δy is directly related to the change in phase $\Delta\varphi$ between the Tx and Rx using Equation (1) [39].

$$\Delta y = \frac{\Delta\varphi}{2\pi}\frac{\lambda}{2} \tag{1}$$

By using elliptical fitting and arctangent modulation, raw radar data (I and Q components) was converted into single-channel radar data, which was then digitized by a 24-bit Analog to Digital Converter (ADC). The segmentation network based on 1D-CNN is the core component of the framework presented in Fig. 2(ii). Before using the input data in the segmentation network, the proposed framework incorporates a preprocessing module that performs cleaning, converting, and normalizing operations on the input data. A critical step is ensuring that the data are formatted in a manner that is compatible with the model and minimizing any outliers or noises. In the next step, the preprocessed data is fed into the 1D segmentation model, which detects certain properties in the radar signal that correspond to different segments and then uses these features to generate ECG waveforms. This network consists of several layers of neural networks that analyze incoming data, identify notable characteristics, and provide predictions. As shown by previous studies [42–46] one-dimensional segmentation is one of the most well-established approaches for domain transformation or signal synthesis in the signal processing literature. This output is then fed into a post-processing module based on the 1D-CNN segmentation network. Based on the network's predictions, this module calculates several performance metrics and evaluates the effectiveness of the proposed framework using the provided "ground truth" ECG.

Preprocessing of radar data and ECG waveforms is necessary in order to prepare them for DL. A 5-fold cross-validation is performed on the processed data by dividing it into train, test, and validation sets.

2.2. Dataset description

A radar benchmark dataset [33] contains raw radar signals (radar In-phase (I) and Quadrature (Q) components) and corresponding "reference ground truth" ECG signals. In this study, signals were obtained from 30 test subjects in five different scenarios over 24 h. This dataset is used for training and testing the proposed ECG pattern estimation framework. A meticulously planned methodology was used by the Department of Palliative Medicine at University Hospital Erlangen to collect data. There are 30 healthy individuals in the dataset, 14 of whom are men and 16 of whom are women. The average age of the participants is 30.7 $\pm$ 9.9 years, and their average Body Mass Index (BMI) is 23.2 $\pm$ 3.3 kg/m^2. An ECG is used during the tests to record the heart's electrical activity [33]. Using the clinical protocol, the four leads are connected as follows: the right arm lead is coded in red, the left arm lead is coded in yellow, the left leg lead is coded in green, and the right leg lead is coded in black. A new set of gel electrodes was provided to each individual. Using Einthoven's triangle [47], the TFM (Task Force Monitor) collected raw information from leads 1 and 2. The software analyzes and generates these additional ECG leads, but it does not record or include the data for leads 3 and the augmented limb leads in the output file in.mat format. The ECG channels are converted into digital form at the TFM using a sampling rate of 2000Hz and a precision of $\pm 5\mu V$.

Throughout the Rest scenario, subjects maintained consistent and regular breathing rhythms while relaxed. Monitoring the combined I/Q components of the radar as well as the ECG during the Resting situation required a minimum of 10 min for each test participant. A Valsalva technique was performed consecutively, which involves forcefully

exhaling while keeping the glottis closed for 20 s [48]. In the experiment, the Valsalva technique was repeated three times with a 5-min break in between. In the sleep Apnea experiment [49], the participants intentionally refrained from breathing for as long as they could under two conditions. In the first phase, participants breathed deeply before holding their breath. In the next phase, participants exhaled thoroughly before holding their breath. The participants in both conditions were voluntarily triggered to perform the intervention by holding their breath while pressing a button. It is important to emphasize that not all participants participated in all radar and ECG data collection situations. Data was collected from all 30 test participants during the Resting scenario, 27 test subjects during the Valsalva scenario, and 24 test participants during the Apnea scenario. A combined image of raw radar signals (consisting of in-phase and quadrature components), radar data (obtained from both I and Q components), and corresponding ground truth ECGs is shown in Fig. 3.

2.3. Data preprocessing

The preparation of data is one of the most crucial and essential stages of DL systems. Before using the data in a DL pipeline, the data has to be cleansed, aligned, standardized, and segmented. The processes ensure that the data is in a format that can be used by the model effectively and that any outliers or mistakes, such as NaN or infinite numbers, are removed. The performance of a model can be greatly enhanced by organizing and pre-analyzing data optimally. In this research, the signals were resampled, baseline drift corrected, filtered, segmented windowed, and normalized. The following subsections provide detailed descriptions of each of these concepts.

2.3.1. Resampling

In the data collection phase, the raw radar signals and the ground truth ECG signals were sampled at 2000 Hz. In this study, radar data and ECG signals were down-sampled from 2000 to 128 Hz. As long as a suitable decimation technique is used, followed by low-pass filtering [50], down sampling does not significantly affect a signal's shape. During this study, linear interpolation was found to be suitable for reducing the number of data points in the waveforms.

2.3.2. Notch and bandpass filtering

The notch filter effectively removes frequencies from signals. Under certain conditions, it helps digest radar signals. In a notch filter, certain frequency bands are suppressed while others are allowed to pass through. The filter's intended function is to attenuate the amplitude of frequencies in the range of 50/60 Hz, which are frequently related to power line interference [51]. Higher filter orders reduce notches and attenuate target frequencies more effectively. Considering the importance of avoiding power line interference, a moderate to high filter order can be used to minimize signal distortion while attenuating unwanted frequencies. By progressively linking high-pass and low-pass filters, notch filters eliminate power line noise. Power line frequencies must match the cutoff frequencies of these filters. The use of bandpass filters is essential for the analysis of ECGs. Filter order determines the sharpness of the transition between passband and stopband in a bandpass filter. ECG signal components may be isolated while noise and interference are reduced by using higher filter orders, which may improve selectivity and roll-off. Heart rate, breathing rate, and ECG signal components are included in this range. A Halter filter with a passband of 0.5–40 Hz was used to process the ground truth ECG data. By reducing powerline interference and targeting ECG and respiration rate frequencies, the Halter filter tailors data processing to each patient's needs. A comparison between the Halter filter and bandpass filtering techniques will help determine the quality of the signal and how much distortion it reduces. Contrary to high-order bandpass filters, the Halter filter balances noise reduction and signal preservation. In this present work, Halter filters are tested visually, statistically, and clinically to ensure appropriate parameter selection and signal integrity.

2.3.3. Baseline drift correction

A baseline drift correction method is used to eliminate undesired fluctuations in a signal's baseline. Several factors can cause baseline drift in time-series data, such as fluctuations in temperature, humidity, and equipment. DL models may be adversely affected by baseline drift, making it difficult to extract valuable information from signals. Several methods are available for correcting baseline drift in one-dimensional signals, including moving average filters, wavelet transforms, and polynomial fitting. Based on segments of radar and ECG data, polynomial fitting is applied to eliminate baseline wander using MATLAB. Based on [52,53], a polynomial of order 5 was found to be suitable for eliminating baseline drift.

2.3.4. Segmentation or windowing

The performance of a DL model tends to be improved by using shorter segments of raw radar signals and ECG signals. Longer segments may contain information that might be missed during training by the model. Furthermore, shorter windows would reduce the amount of processing resources required during the training phase. The radar signal and the ground truth ECG were divided into segments, with each segment containing 1024 sample points, as outlined in previous research [45,54]. The model's performance and segmentation number were enhanced by utilizing a 50 % overlap during the segmentation phase of the train set specifically. The method is similar to the patching technique often used in image processing [55]. Using overlapping sections and segmenting the signals into smaller sections increases the performance of the model and reduces training computing resources.

2.3.5. Normalization

It is essential to normalize input data in DL to ensure that scaling doesn't negatively affect the performance of the model. All input characteristics are equally important, limiting the dominance of large-scale features during training. Additionally, normalization speeds up the convergence of the model by reducing the variability of the input data. As a result, it increases training effectiveness as well as a model's ability to apply knowledge to new data and reduces overfitting, which occurs when a model learns noise instead of underlying patterns. In general, normalization facilitates the training of DL models consistently and efficiently. Data normalization simplifies the input data and prevents overfitting by lowering its complexity. To process the segments of radar signals and ground truth ECG signals, "Z-score" and "range normalization" techniques were used (Equation (2)). Through Z-score normalization, the data was transformed to have a mean of zero and a standard deviation of one. Standardizing signals with large variations is advantageous with this approach. A range normalization was used to restrict amplitudes to a zero to one range. DL algorithms benefit from this because it ensures that the model is not influenced by input data scale, and that all input characteristics have equal importance [42].

$$Signal_k(norm) = range\left(\left(\frac{Signal_k - \mu_k}{\sigma_k}\right), [0\ 1]\right) \tag{2}$$

2.4. Overview of the proposed MultiResLinkNet

The purpose of this section is to examine the complexities of the proposed MultiResLinkNet, a DL model specifically designed to synthesize ECG data from 1D segmentation network using radar signals. The MultiResLinkNet architecture integrates LinkNet [36] and MultiResUNet [56] achievements in 2D-segmentation tasks. Unlike UNet [35], LinkNet incorporates residual blocks rather than regular convolution layers and merges skip connections from the decoder layers using addition rather than stacking. In each layer, addition does not increase the feature dimension, as opposed to concatenation or stacking. In addition, the feature vectors are altered according to the connections

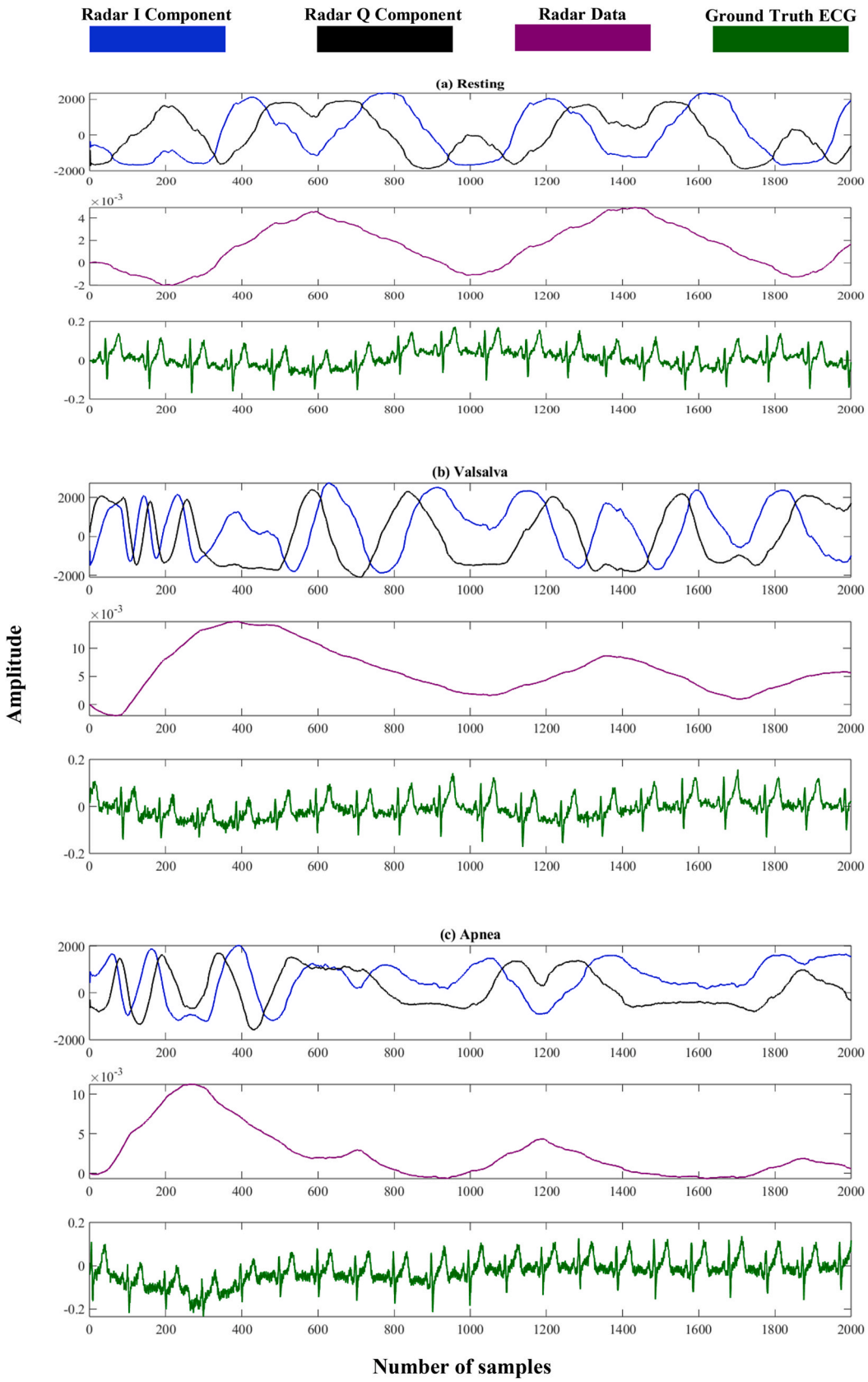

Fig. 3. Illustration of radar signal (I and Q components), radar data (generated from I and Q components) and corresponding ground truth (GT) ECG (ECG) waveforms in (a) Resting (b) Valsalva (c) Apnea scenarios.

made by the encoders. It is, however, essential that the feature maps align precisely in every dimension in order to add them. Modifying the feature maps in order to precisely align them with one another may sometimes be necessary. We replace the convolution blocks of LinkNet with Multi-Residual blocks from MultiResUNet (Fig. 4(b)) along with intra-layer residual connections, as shown in Fig. 4(a). MultiRes blocks effectively extract characteristics from the dataset in varying levels of detail. We can also use Residual Paths or ResPaths [56] instead of direct skip connections from encoder levels (see Fig. 4(c)). As shown in Fig. 4 (a), these ResPaths are added to the deeper decoder layer features. A ResPath handles the characteristics from the encoder layers before including them, which is absent from direct skip connections. A bottleneck layer is not present in MultiResLinkNet, as in LinkNet. Using auxiliary outputs, we closely monitor each encoder layer and improve the intermediate layers to improve the network's performance.

3. Experiment setup and performance metrics

In the following part, the experimental approach used in this study is thoroughly described, including all necessary elements employed in this study. In addition, the evaluation metrics that were used in this work are described in a separate section. Based on these metrics, we can objectively evaluate the performance of deep CNN models applied to the synthesis of ECG waveforms from single-channel radar signals. MultiResLinkNet and three other 1D-CNN models (Feature Pyramid Network (FPN) [56], UNet [35], and LinkNet [36]) underwent extensive end-to-end training. Normalized radar signals (known as 'x') and their matching ground truth ECG segments (known as 'z') were input into neural networks during the training process. This DL model's primary objective was to gain knowledge of a nonlinear function capable of efficiently transferring 'x' to 'z'. As a loss function, the mean square error (MSE) function was used to construct the intended nonlinear mapping in order to enhance this process of acquiring knowledge. By using gradient descent, we decreased the variation between the synthesized and ground-truth segments. In this case, we optimized the loss function via the Adam optimizer, at a constant learning rate ($\alpha = 0.0005$). The data were divided into a training set, comprising 80 % of the total data, and a test set, comprising 20 % of the total data. Furthermore, 20 % of the training data was utilized for validation. It is important to emphasize that separate test subjects were used for dividing the train, test, and validation sets, ensuring that no data was shared among them. The four networks were trained, validated, and tested independently using the five-fold cross-validation technique within the Google Colab Pro computing environment. Sub-sections 3.1 and 3.2 describe the two experiments involved in this study, whereas sub-section 3.3 describes the metrics used for assessing the performance of the DL models.

3.1. Experiment A

As part of Experiment A, the following three scenarios were considered separately: resting, Valsalva, and apnea. According to each scenario, radar segments were input as predictor signals into the 1D segmentation model, and ground truth ECG segments, which the model needed to synthesize, were provided as target signals. As a result, all three models had a single input channel and a solitary output channel. In addition to MultiResLinkNet, we trained and tested three other cutting-edge 1D segmentation networks: FPN, UNet, and LinkNet. All network parameters were standardized to maintain integrity. In this context, various parameters are taken into account, including the number of layers, depth, filters, and kernels within each layer, width, etc. There were 5 layers in each model, with an initial layer containing 64 filters, which were then doubled in subsequent layers. The momentum factor is determined indirectly by the 'beta_1′ parameter, which signifies the exponential decay rate for the initial moment estimates, in the Adam optimizer configuration provided. The default value of 'beta_1′ is commonly set to 0.9. In MaxPooling2D layer setup, the stride factor, controlled by the strides parameter, specifies the pooling step size along the input data's vertical and horizontal dimensions. Strides of (2, 2) shift the pooling procedure by 2 steps in both dimensions, altering output feature map spatial dimensions and training computing efficiency. The Google COLAB Pro platform was used to train each model with 300 epochs and a specified epoch patience of 20. Across three distinct scenarios, the number of segments created varied due to differences in recording time and the number of participants. Specifically, the dataset includes data from all 30 test participants, totaling 19048.6 s in the

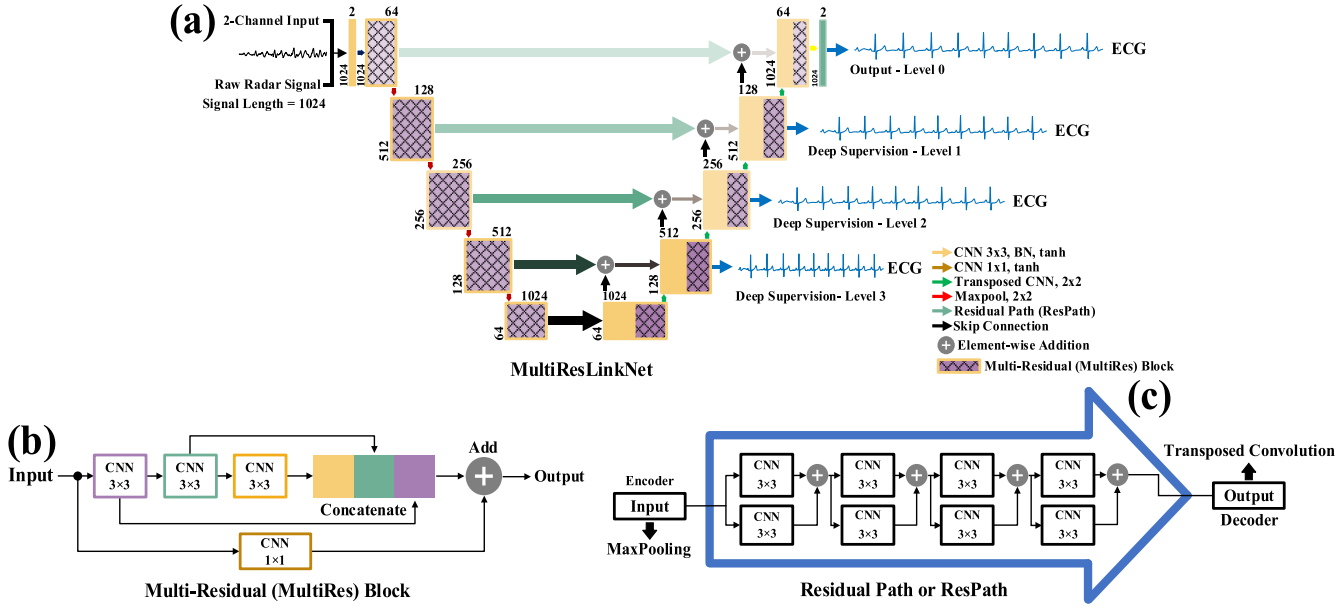

Fig. 4. Illustration of the constructed MultiResLinkNet. The Figure describes three components: (a) the MultiResLinkNet design, (b) the Multi-Residual (MultiRes) block, and (c) the enlarged Residual Path or ResPath. MultiResLinkNet differs from MultiResUNet by using feature addition instead of concatenation via the ResPaths, resulting in a lighter and computationally less intensive model.

Resting condition. A total of 27 and 24 test participants were available for the Valsalva and Apnea situations, respectively. During the Valsalva scenario, the recording lasted 27968.3 s, while during the Apnea scenario, it lasted 4705.2 s. Data from both the train and test sets are presented in Table 1, showing the number of segments acquired from three different situations. This experiment aims to determine how well DL models synthesize radar signals (from radar to ECG).

3.2. Experiment B

In the second experiment, the emphasis is more on practical application than in the previous experiment. It is not possible to completely restrict the patient's mobility because the test subject is likely to assume various positions during prolonged and continuous monitoring. As a result, the DL model must have high levels of resilience to generate ECG signals precisely under a variety of circumstances. As a result, the research endeavor is driven primarily by this motivation. Data from all three scenarios (Resting, Valsalva, Apnea - RVA) were aggregated and a 1D segmentation network was trained. Using the same approach as in experiment A, subject-wise stratification was used in experiment B, instead of random stratification, to ensure that there was no data leakage between the train and test sets. A five-fold cross-validation procedure was again applied and the same four 1D CNN models were deployed. We carefully created training and test sets in a controlled environment for our second experiment. Our training set was created by integrating 80 % of the radar data with the ground truth ECG segments for each condition. Similarly, the test set consisted of the remaining 20 % of radar segments and their associated ground truth ECG segments. There were a total of 12,794 segments created, with 10,236 segments being the training set and 2558 segments being the test set. There is a primary difference between experiments A and B in the data used. As part of experiment A, we trained and tested our DL models using particular scenarios. It is important to note that these models may not perform optimally when tested with data from diverse situations. Comparatively, experiment B involved training DL models using data from three different scenarios, which resulted in improved generalization. It is expected that models trained using this method will exhibit greater resilience when evaluated using radar segments illustrating multiple stances. In real-world scenarios, the subject probably being tested will assume different stances, resulting in different radar signals across different scenarios.

3.3. Performance metrics for quantitative evaluation

Several established performance metrics are used to evaluate the effectiveness of the four DL models in synthesizing ECGs from radar data. In both temporal and spectral domains, these metrics include Mean Absolute Error (MAE), Mean Squared Error (MSE), Temporal Correlation Coefficient ($CC_{temporal}$), Spectral Correlation Coefficient ($CC_{spectral}$), and Relative Root Mean Squared Error (RRMSE) (Equations (3)–(8)) [42,46]:

$$MAE = \frac{\sum_{i=1}^{M}\left(\frac{\sum_{j=1}^{N}\left|z_{ij}-\widehat{z}_{ij}\right|}{N}\right)}{M} \tag{3}$$

Table 1
The quantity of segments obtained from radar data and the corresponding ground truth ECG for the train and test sets in experiment A.

Scenario	Total Subjects	Total Segments	Train Set (80 %)	Test Set (20 %)
Resting	30	4702	3762	940
Valsalva	27	6952	5562	1390
Apnea	24	1140	912	228

$$MSE(z) = \frac{\sum_{i=1}^{M}\left(\frac{\sum_{j=1}^{N}\left(z_{ij}-\widehat{z}_{ij}\right)^2}{N}\right)}{M} \tag{4}$$

$$CC_{temporal} = \frac{Cov(z,\widehat{z})}{\sqrt{Var(\widehat{z})\cdot Var(z)}} \tag{5}$$

$$CC_{spectral} = 100\left(1-\frac{1-\rho(PSD(\widehat{z}),PSD(G_{x2C}(\widehat{z})))}{1-\rho(PSD(\widehat{z}),PSD(z))}\right) \tag{6}$$

$$RRMSE_{temporal} = \frac{RMS(\widehat{z}-z)}{RMS(z)} \tag{7}$$

$$RRMSE_{spectral} = \frac{RMS(PSD(\widehat{z})-PSD(z))}{RMS(PSD(z))} \tag{8}$$

$$Pearson\ Correlation\ Coefficient, \rho(x,y) = \frac{\sum_{i=1}^{n}(x_i-\overline{x})(y_i-\overline{y})}{\sqrt{\sum_{i=1}^{n}(x_i-\overline{x})^2}\sqrt{\sum_{i=1}^{n}(y_i-\overline{y})^2}} \tag{9}$$

Where, z and $\widehat{z}$ represent ground truth and estimated ECG segments, respectively. In this research, 'N' represents the 1024 time-domain data points per segment. In this research, 'N' refers to the 1024 time-domain data points per segment. In Table 1, 'M' represents the total number of segments in a scenario. A covariance metric is used (Cov), a variance metric is used (Var), and a power spectrum density metric is used (PSD) based on the periodogram calculations [57]. Implementing $CC_{Spectral}$ involves employing the Pearson Correlation Coefficient (ρ or PCC) [58], as shown in Equation (9). The MAE and MSE are often used in machine learning to assess prediction models [42,43,54]. MAE is important because it provides an interpretable way to measure the correctness of a model. An MAE evaluates the average magnitude of errors in a collection of predictions without considering their direction, so it can determine the average difference between expected and actual values regardless of forecast overestimation or underestimation. MSE provides a clear and consistent measure of model accuracy that is sensitive to the size of prediction errors. Based on average squares of differences between expected and actual values, MSE gives more weight to larger mistakes and shows the total deviation of predictions from actual values. As a result, lower MAE and MSE indicate better performance. Two signals are compared using the correlation coefficient to determine their linear similarity in the time domain. Correlation values of −1 indicate a perfect negative linear connection, 1 indicates a perfect positive linear connection, and 0 indicates no linear connection. In the frequency domain, the correlation coefficient measures coherence and linear connection between two signals. It can be used to find common frequencies by showing signal frequencies. Correlation coefficients above 0.80 suggest signal similarity, which is always predicted in prediction cases. The RRMSE measures the difference between two signals based on their time and frequency domains, respectively. A lower RRMSE indicates better performance.

This study also calculates Accuracy, Precision, Recall, and F1-score by detecting the ECG peak from the predicted/synthesized and corresponding ground truth ECGs.

$$Accuracy = \frac{TP+TN}{TP+TN+FP+FN} \tag{10}$$

$$Precision = \frac{TP}{TP+FP} \tag{11}$$

$$Recall = \frac{TP}{TP+FN} \tag{12}$$

$$F1\ Score = 2 * \frac{Precision * Recall}{Precision + Recall} \tag{13}$$

Accuracy is the percentage of True Positives (TP) and True Negatives (TN) predicted correctly across all occurrences. The precision of a model measures its accuracy in optimistic predictions. In this calculation, the True Positives are divided by the total number of positive predictions (correct and incorrect). Alternatively, recall can be described as sensitivity or true positive rate as it measures how well a model can recognize positive events from all positive ones. In F1 Score, precision and recall are balanced. In this way, the harmonic mean of accuracy and recall is calculated to calculate a single score, which measures the precision and accuracy of positive predictions.

Furthermore, the Mean R–R interval (μ_{RR}), heart rate (μ_{HR}; calculated as beat per minute), The standard deviation of heart rate (σ_{HR}), and Root mean square of consecutive RR interval differences (RMSSD) is also calculated for the predicted and ground truth ECG using Equations (14)–(16) [59]:

$$\mu_{RR} = \frac{\sum_{i=1}^{N-1} T_{RR}(i+1) - T_{RR}(i)}{N-1} \tag{14}$$

$$\sigma_{HR} = \frac{\sum_{i=1}^{N} HR(i) - \mu_{HR}}{N-1} \tag{15}$$

$$RMSSD = \sqrt{\frac{\sum_{i=1}^{N} (T_{RR}(i+1) - T_{RR}(i))^2}{N-1}} \tag{16}$$

Where, the mean R–R interval (μ_{RR}) is the average time between two consecutive ECG peaks, measured in milliseconds.

Equation (14) defines μ_{RR} by defining R peaks as N and R-peak time as T_{RR}. The heart rate fluctuates within a certain range rather than beating at a constant pace. The standard deviation of heart rate (σ_{HR}) quantifies the extent to which heart rate varies from the anticipated value (Equation (15)). Typically, it is quantified in bits per minute (bpm). The RMSSD is a widely used measure for heart rate variability (HRV) (Equation (16)). It is computed by summing the squared RR interval differences and then finding the square root of the result.

3.4. Qualitative evaluation

In many cases, quantitative metrics are considered adequate for evaluating the performance of a system. Visual comparisons are essential for persuading ordinary readers or non-technical corporate executives. We qualitatively evaluate each experiment by comparing sample ECG waveforms derived from radar data with corresponding ground truth ECGs. It is important to point out that generative ECGs were evaluated by individuals with particular cardiac physiology expertise to compare to ground truths. As a result, we made precise correlations between the anticipated and authentic electrocardiogram (ECG) segments using our expertise in the field of electrocardiogram (ECG) signals. To ensure precise alignment, we used a visual representation of the process, focusing on our understanding of ECG signal. The plots in Section 4 have been created separately for each experiment and DL model tested.

4. Results and discussion

This section presents the findings of two experiments and conducts a thorough analysis of the outcomes with qualitative examples (where applicable).

4.1. Results of experiment A

In Table 2, the results of experiment A are presented under three scenarios of radar data: resting, Valsalva, and apnea. Figs. 5–7 are qualitative results for the aforementioned scenarios using the models FPN, UNet, LinkNet, and MultiResLinkNet.

A comparison of the proposed MultiResLinkNet model with the other three DL models reveals that it produces the highest average temporal and spectral correlation coefficients in Resting, Valsalva, and Apnea scenarios, the lowest MAE in Resting, the lowest MSE in Apnea, and the lowest $RRMSE_{temporal}$ and $RRMSE_{spectral}$ values in all three scenarios (Table 2).

According to the higher estimated performance metrics, it is apparent that our proposed model is capable of generating ECG waveforms from radar segments in the scenarios mentioned above. The LinkNet has demonstrated the best performance in Resting with a Mean

Table 2
Performance measurements during Resting, Valsalva, and Apnea scenarios, separately.

Scenario	1D Segmentation Model	MAE ± STD	MSE ± STD	Average Temporal Correlation Coefficient ± STD	Average Spectral Correlation Coefficient ± STD	Temporal RRMSE ± STD	Spectral RRMSE ± STD[a]
Resting	FPN	0.14204 ± 0.06	0.03170 ± 0.02	58.37370 ± 18.21	71.37612 ± 22.80	0.46940 ± 0.22	0.73374 ± 0.26
	UNet	0.13872 ± 0.07	0.03219 ± 0.02	63.10263 ± 20.43	74.68087 ± 23.17	0.45760 ± 0.23	0.86096 ± 0.64
	LinkNet	0.13588 ± 0.06	**0.03034 ± 0.02**	64.34710 ± 19.20	74.37377 ± 23.40	0.45116 ± 0.23	0.81111 ± 0.55
	MultiResLinkNet	**0.13258 ± 0.07**	0.03066 ± 0.02	**66.09523 ± 19.33**	**82.43880 ± 18.42**	**0.43682 ± 0.22**	**0.71412 ± 0.50**
Valsalva	FPN	**0.14985 ± 0.07**	**0.03679 ± 0.03**	57.53041 ± 21.80	65.96767 ± 26.42	0.46395 ± 0.18	0.87990 ± 0.59
	UNet	0.15249 ± 0.08	0.03928 ± 0.03	58.38068 ± 21.77	68.78898 ± 26.31	0.46553 ± 0.19	0.99554 ± 0.88
	LinkNet	0.15087 ± 0.08	0.03869 ± 0.03	56.62680 ± 22.58	66.86613 ± 27.02	0.46195 ± 0.18	0.99095 ± 0.85
	MultiResLinkNet	0.15286 ± 0.08	0.04012 ± 0.04	**60.13625 ± 21.92**	**77.05186 ± 23.26**	**0.46083 ± 0.19**	**0.80660 ± 0.69**
Apnea	FPN	0.15310 ± 0.06	0.03853 ± 0.03	39.11945 ± 18.67	51.26071 ± 28.35	0.51017 ± 0.22	1.00889 ± 0.48
	UNet	**0.14406 ± 0.06**	0.03495 ± 0.02	56.14069 ± 18.38	69.97450 ± 25.05	0.47825 ± 0.21	0.92034 ± 0.48
	LinkNet	0.14572 ± 0.06	0.03526 ± 0.02	**56.22281 ± 18.99**	70.34953 ± 24.98	0.47944 ± 0.19	0.91749 ± 0.56
	MultiResLinkNet	0.14474 ± 0.06	**0.03474 ± 0.02**	55.33149 ± 18.95	**74.65785 ± 23.17**	**0.47692 ± 0.20**	**0.82392 ± 0.45**

[a] STD: Standard deviaion.

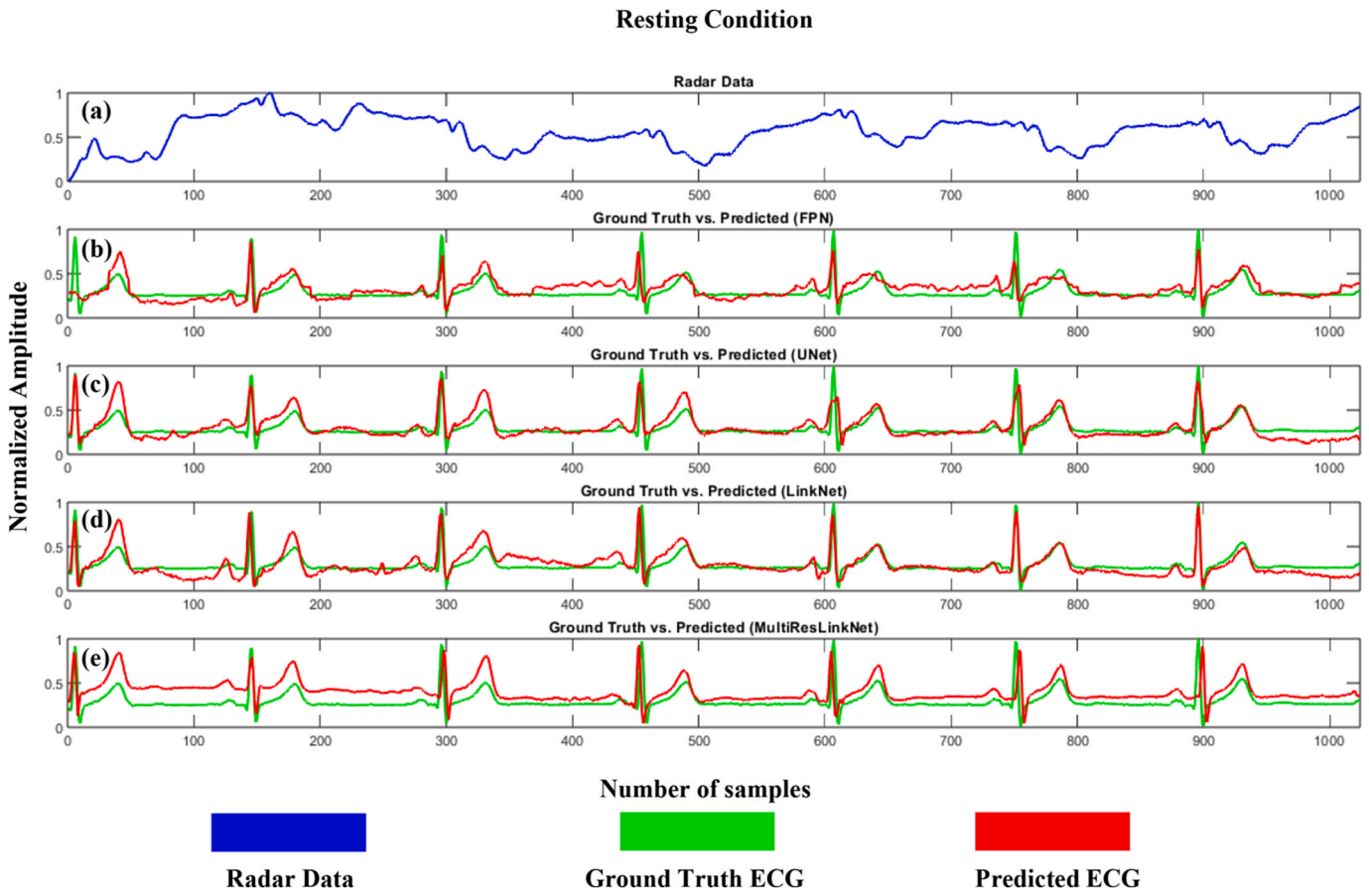

Fig. 5. An instance of synthesized ECG segment utilizing (b) FPN, (c) UNet, (d) LinkNet, and (e) Our proposed MultiResLinkNet in the Resting scenario. In the uppermost subplot (a), the radar data is illustrated.

Squared Error value of 0.03034 ± 0.02. FPN achieved the greatest performance in the Valsalva scenario with MAE values of 0.14985 ± 0.07 and MSE values of 0.03679 ± 0.03. UNet achieved the lowest Mean Absolute Error (MAE) of 0.14406 ± 0.06 for Apnea, whereas LinkNet showed the greatest average temporal correlation coefficient of 56.22281 ± 18.99. Our proposed MultiResLinkNet model showed the lowest construction error of 0.03474 ± 0.02. Overall, our proposed MultiResLinkNet model outperformed the other three networks on most performance measures.

4.2. Results of experiment B

As part of Experiment B, we combined data from different scenarios (RVA combined) to map ECG waveforms in a dynamic context from radar segments. A summary of the quantitative findings from Experiment B can be found in Table 3. As shown in Fig. 8, four different 1D CNN models are represented by a segment of radar and a projected ECG.

All four DL models (FPN, UNet, LinkNet, and MultiResLinkNet) perform similarly on the combined scenario data. MultiResLinkNet, as proposed, exhibits superior performance as evidenced by its average temporal correlation coefficient of 61.86265 ± 21.37 and average spectral correlation coefficient of 79.96201 ± 20.82. Further, it has the highest temporal RMSE of 0.44618 ± 0.17 and the highest spectral RRMSE of 0.73269 ± 0.56. In contrast, the FPN demonstrated the lowest MAE and MSE values of 0.03422 ± 0.03 and 0.014316 ± 0.07, respectively. With the lowest average temporal correlation coefficient (57.64728 ± 22.17), the lowest average spectral correlation coefficient (68.38843 ± 26.54), and the highest spectral RRMSE (0.94118 ± 0.75), UNet performed the least well out of the three 1D segmentation networks examined.

It is evident from Tables 2 and 3 that our MultiResLinkNet model is the most effective method of synthesizing ECG from single-channel radar data, with the highest temporal and spectral correlation coefficients, as well as the lowest RRMSE. Accordingly, in comparison to other established models, our MultiResLinkNet model, in its proposed form, is more capable of acquiring knowledge about a wide array of features from the radar data and synthesizing ECGs as effectively as possible.

Incorporating DL models into the synthesis of radar-based ECGs eliminates any physical contact with the patient; as a result, the process is completely non-contact and non-invasive. As a result, this methodology represents a more secure and pleasant option for prolonged patient observation, especially in intensive care units catering to surgical patients. The framework we propose can also be easily modified to provide continuous and real-time data for a prolonged period, a capability that is beyond the capabilities of traditional intermittent measurement methods. As a result, patients can be monitored for extended periods using ECGs. As radar devices advance, a variety of settings, including residences and hospitals, are capable of being monitored wirelessly and by portable sensors. It is hoped that our radar-based ECG monitoring framework might provide a more affordable solution compared to conventional approaches requiring constant sensor replacement, invasive procedures, and multiple devices.

4.3. ECG peak detection matrices

In our study, we used a variety of ECG detectors, including Hamilton, Pan Tompkins, Stationary Wavelet Transform (SWT), Engzee, Threshold-based, Christov, WQRS, and "Two Average" methods. These detectors detect ECG peaks from synthesized ECG signals predicted by

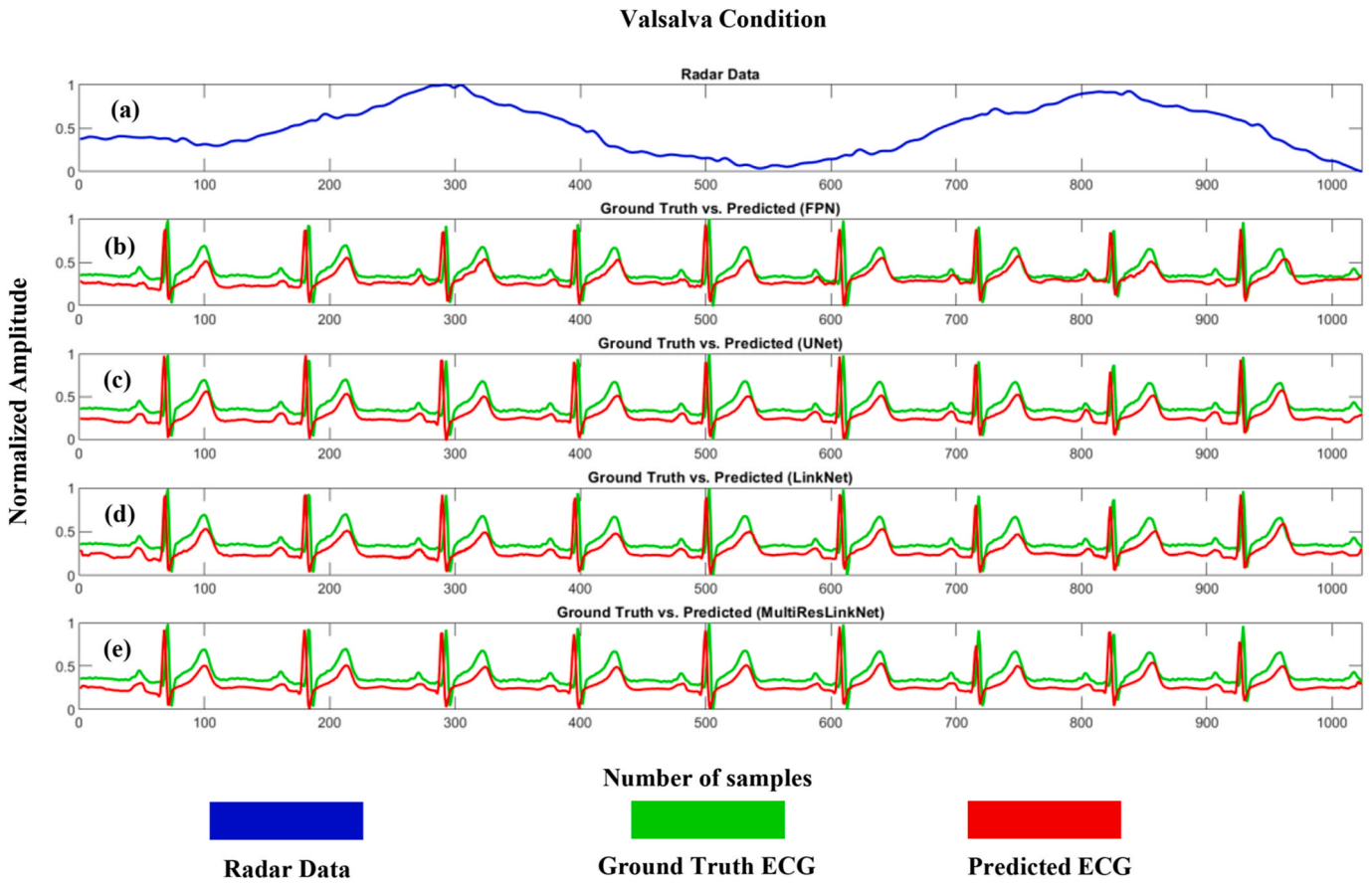

Fig. 6. An instance of predicted ECG segment utilizing (b) FPN, (c) UNet, (d) LinkNet, and (e) Our MultiResLinkNet model as proposed in the context of the Valsalva scenario. In the uppermost subplot (a), the radar data is illustrated.

the MultiResLinkNet model. In terms of the various methods considered, the "Two Average" approach is selected due to its exceptional performance across multiple detection criteria, including Accuracy, Precision, Recall, and F1-score, in comparison to the alternative detectors utilized in the study. In Table 4, we show the performance metrics for detecting ECG peaks from synthesized ECGs for four scenarios: resting, Valsalva, apnea, and RVA combined. As shown in Table 4, accuracy, precision, recall, and F1 scores are highest for the resting scenario and lowest for the apnea scenario.

Table 5 presents a comprehensive comparison of the predictive and ground truth ECG where μ_{RR}, σ_{RR}, μ_{HR}, σ_{HR}, and RMSSD are computed. The table provides a comprehensive evaluation of the accuracy of the predictions by including both the ground truth and predicted values for each scenario. As evident from Table 5, the predicted values approximate the actual values with minor deviations. The closely matched values of μ_{RR}, σ_{RR}, μ_{HR}, σ_{HR}, and RMSSD computed from synthesized ECG and ground truth ECG signifies that our proposed segmentation model (MultiResLinkNet) is efficient in synthesizing the ECG.

5. Limitations and future directions

We achieved very good results in synthesizing ECG signals from radar signals. However, it is essential to remember that this technology is still in the early stages of development and requires further study to evaluate its effectiveness, dependability, and accuracy when compared to conventional methods. It is apparent from Supplementary Fig. 1S that the radar signal has picked up some mechanical signal related to the heart's electrical activity at the moment of the heart's main electrical activity (i.e., QRS complex). Therefore, the DL model is learning to convert the mechanical signal to the electrical signal of an ECG, which is not a difficult task.

In this assessment, the quality and quantity of data used in training the model are vitally important. It is necessary to use high-quality and varied datasets that cover the situations and settings in which the radar system will be used in order to achieve improved and reliable performance. An accurate synthesis requires a large and diverse dataset, emphasizing both the importance of quantity and variety. A further study could explore other DL models such as Generative Adversarial Networks (GANs) to improve ECG signal quality. Currently, the proposed framework provides only an approximation of ECG patterns. Developing new network designs is essential to further improving performance parameters. By experimenting with new neural network architectures like RNNs, CNNs, or attention mechanisms, the model may be able to recognize complex data patterns and connections. The use of transfer learning and meta-learning may also be used to enhance the ability of pre-trained algorithms to predict ECG signals. In the process of data annotation, manual annotations are crucial to generating accurate signals, emphasizing the need for meticulous attention to detail. Data annotation involves categorizing signal properties such as pulse start and offset or abnormal cardiac rhythms accurately. The annotations serve as ground truth labels for training and evaluating the model in order to generate signals that mimic real-world data.

6. Conclusion

Monitoring an ECG continuously aids in identifying and preventing cardiovascular diseases. Electrodes placed on the body are traditionally used to assess cardiac electrical activity. In this approach, skin irritation, pain, and motion artifacts and interference may occur. In some cases, the patient's movement may be limited, which requires proper setup and

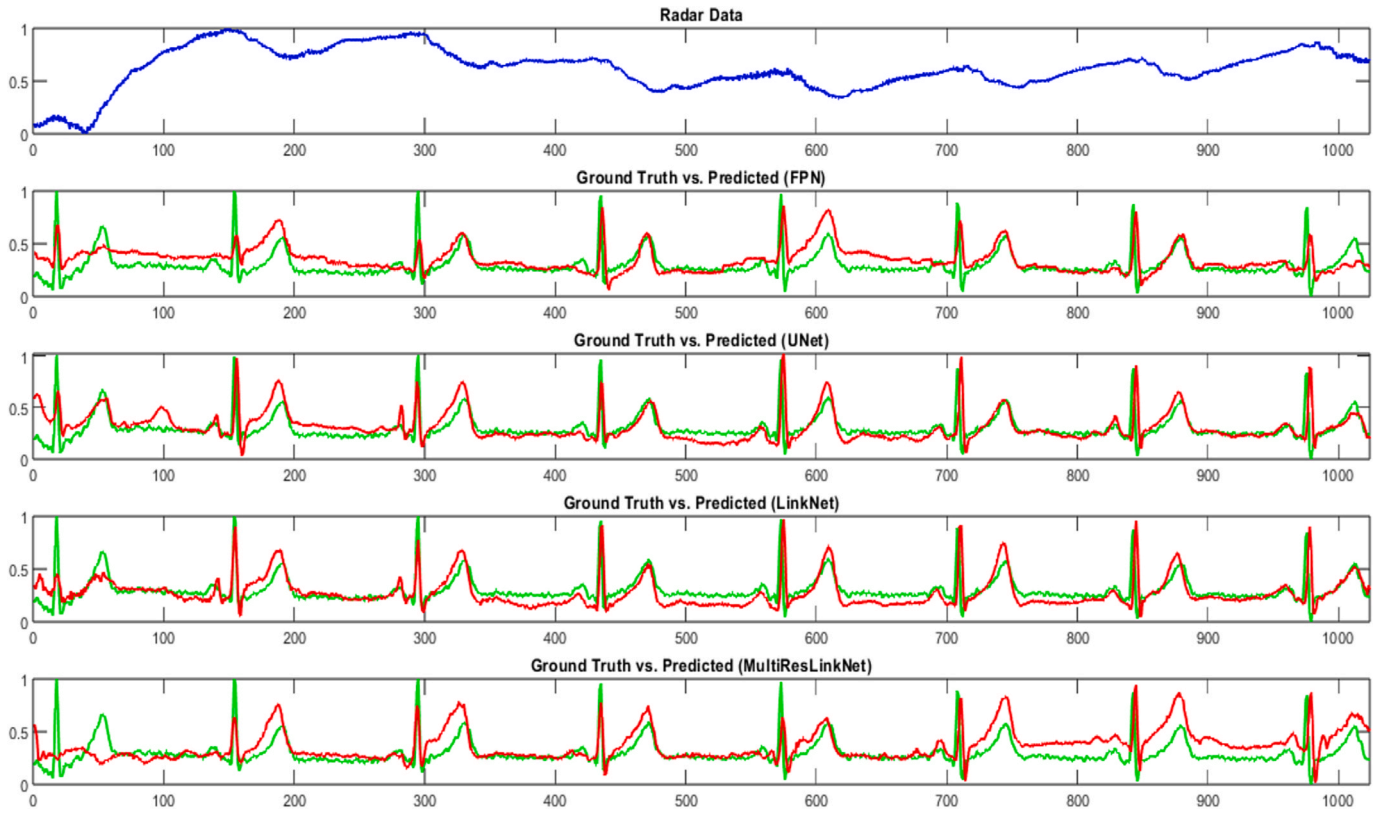

Fig. 7. An instance of estimated ECG segment utilizing (b) FPN, (c) UNet, (d) LinkNet, and (e) Our MultiResLinkNet model as proposed in the context of the Apnea scenario. In the uppermost subplot (a), the radar data is illustrated.

Table 3
Performance metrics for combined scenarios data.

Scenario	1D Segmentation Model	MAE ± STD	MSE ± STD	Average Temporal Correlation Coefficient ± STD	Average Spectral Correlation Coefficient ± STD	Temporal RRMSE ± STD	Spectral RRMSE ± STD[a]
RVA combined	FPN	**0.14316 ± 0.07**	**0.03422 ± 0.03**	59.63209 ± 20.02	69.53405 ± 24.62	0.44694 ± 0.17	0.83026 ± 0.54
	UNet	0.14798 ± 0.08	0.03741 ± 0.03	57.64728 ± 22.17	68.38843 ± 26.54	0.45315 ± 0.17	0.94118 ± 0.75
	LinkNet	0.14780 ± 0.08	0.03723 ± 0.03	58.68552 ± 20.97	70.91253 ± 24.63	0.45487 ± 0.17	0.86909 ± 0.63
	MultiResLinkNet	0.14841 ± 0.08	0.03793 ± 0.03	**61.86265 ± 21.37**	**79.96201 ± 20.82**	**0.44618 ± 0.17**	**0.73269 ± 0.56**

[a] STD: Standard deviaion.

monitoring. A DL algorithm is introduced in this work that reads ECG waveforms directly from radar data without electrodes. This study aims to present a novel method for reinterpreting ECG waveforms using DL models without electrodes directly from radar data. By using MultiResLinkNet, we present a model that generates ECG signals from raw radar I/Q components. As compared to three conventional models (FPN, UNet, LinkNet), our novel methodology exhibits enhanced performance in diverse scenarios (including Resting, Valsalva, Apnea, and their combinations). Our MultiResLinkNet model outperforms these models on six performance measures, demonstrating its ability to reconstruct ECG waveforms precisely and non-invasively. A variety of circumstances proved that MultiResLinkNet outperformed previous DL networks, demonstrating excellent performance in terms of average temporal and spectral correlation coefficients, mean absolute errors (MAE), mean squared errors (MSE), and relative root mean squared errors (RRMSE). In Resting, Valsalva, and Apnea scenarios, MultiResLinkNet consistently outperforms FPN, UNet, and LinkNet. Our research suggests that MultiResLinkNet may be a viable method for reconstructing ECG waveforms precisely and non-invasively. Continuous ECG monitoring could become a breakthrough, especially when invasive techniques are unfeasible or uncomfortable. It is important to conduct further studies to confirm and improve this method for clinical use, which could lead to more convenient and reliable cardiovascular monitoring systems.

Funding

This work is supported by a High Impact Grant from Qatar University# QUHI-CENG-23/24–216. The statements made herein are solely the responsibility of the authors. The open-access publication cost is covered by the Qatar National Library.

Institutional review board statement

Not applicable.

Informed consent statement

Not applicable.

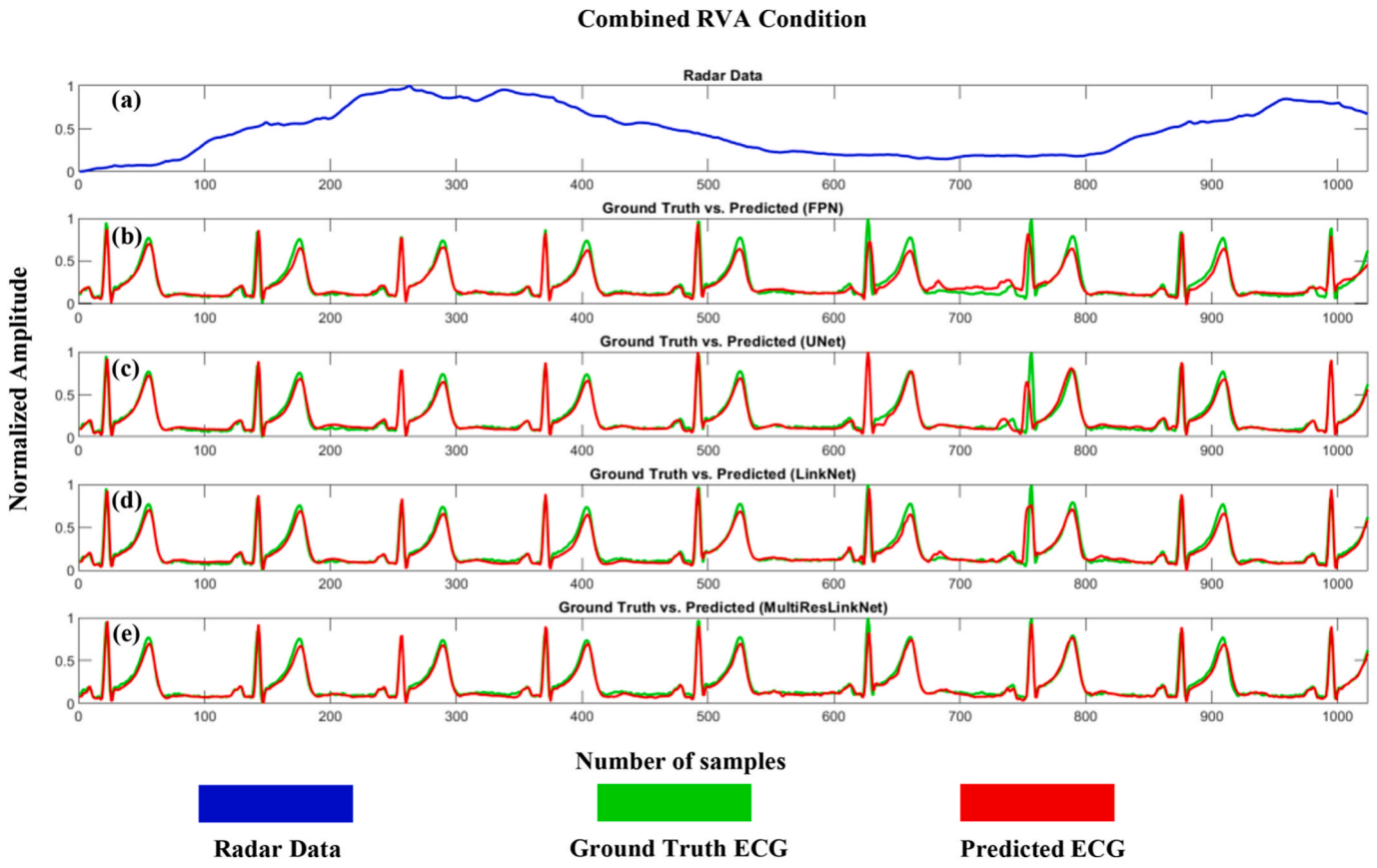

Fig. 8. An instance of synthesized ECG segment utilizing (b) FPN, (c) UNet, (d) LinkNet, and (e) Our MultiResLinkNet model as proposed in the context of all three scenarios data combined. In the uppermost subplot (a), the corresponding radar segment is illustrated.

Table 4
Performance measures in detecting ECG peaks.

Parameters	Resting	Valsalva	Apnea	RVA combined
Accuracy	0.951	0.895	0.799	0.886
F1 Score	0.955	0.944	0.888	0.939
Precision	0.977	0.970	0.939	0.973
Recall	0.934	0.920	0.842	0.908
True Positives	17787	26039	4156	17512
False Positives	409	799	266	482
True Negatives	0	0	0	0
False Negatives	1243	2240	779	1764

Table 5
Compares ground truth and prediction results across physiological scenarios.

Scenario	ECG	μ_{RR} (ms)	σ_{RR} (ms)	μ_{HR} (bpm)	σ_{HR} (bpm)	RMSSD (ms)
Resting	Ground Truth	126.49	19.26	62.12	9.638	12.95
	Prediction	125.71	22.41	63.34	13.72	23.87
Valsalva	Ground Truth	125.79	20.41	62.70	10.56	13.58
	Prediction	125.42	23.34	63.64	13.96	24.08
Apnea	Ground Truth	118.25	19.60	66.72	11.17	13.17
	Prediction	117.81	25.49	68.57	17.05	31.50
RVA	Ground Truth	124.88	21.78	63.79	14.38	14.20
	Prediction	125.71	22.41	63.34	13.72	23.87

CRediT authorship contribution statement

Farhana Ahmed Chowdhury: Writing – original draft, Software, Data curation, Conceptualization. **Md Kamal Hosain:** Methodology, Formal analysis, Conceptualization. **Md Sakib Bin Islam:** Writing – original draft, Visualization, Software, Formal analysis. **Md Shafayet Hossain:** Visualization, Validation, Formal analysis. **Promit Basak:** Writing – original draft, Validation, Software. **Sakib Mahmud:** Writing – original draft, Software, Methodology. **M. Murugappan:** Writing – review & editing, Validation, Supervision, Resources, Conceptualization. **Muhammad E.H. Chowdhury:** Supervision, Resources, Project administration, Funding acquisition.

Declaration of competing interest

Authors have no conflict of interest to declare.

Acknowledgment

The dataset used in this study is kindly shared by Schellenberger et al. [33].

Appendix A. Supplementary data

Supplementary data to this article can be found online at https://doi.org/10.1016/j.compbiomed.2024.108555.

References

[1] A.L. Goldberger, Z.D. Goldberger, A. Shvilkin, Goldberger's Clinical Electrocardiography-E-Book: A Simplified Approach, Elsevier Health Sciences, 2023.

[2] A.I. Taloba, et al., Machine algorithm for heartbeat monitoring and arrhythmia detection based on ECG systems, Comput. Intell. Neurosci. 2021 (2021).
[3] T.W. Bae, K.K. Kwon, ECG PQRST complex detector and heart rate variability analysis using temporal characteristics of fiducial points, Biomed. Signal Process Control 66 (2021) 102291.
[4] R. Costa, T. Winkert, A. Manhães, J.P. Teixeira, QRS peaks, P and T waves identification in ECG, Procedia Comput. Sci. 181 (2021) 957–964.
[5] V. Gupta, M. Mittal, R-peak detection in ECG signal using Yule–Walker and principal component analysis, IETE J. Res. 67 (6) (2021) 921–934.
[6] M. Kebe, R. Gadhafi, B. Mohammad, M. Sanduleanu, H. Saleh, M. Al-Qutayri, Human vital signs detection methods and potential using radars: a review, Sensors 20 (5) (2020) 1454.
[7] N. Malešević, V. Petrović, M. Belić, C. Antfolk, V. Mihajlović, M. Janković, Contactless real-time heartbeat detection via 24 GHz continuous-wave Doppler radar using artificial neural networks, Sensors 20 (8) (2020) 2351.
[8] I. Seflek, Y.E. Acar, E. Yaldiz, Small motion detection and non-contact vital signs monitoring with continuous wave Doppler radars, Elektronika ir elektrotechnika 26 (3) (2020) 54–60.
[9] K. Yamamoto, R. Hiromatsu, T. Ohtsuki, ECG signal reconstruction via Doppler sensor by hybrid DL model with CNN and LSTM, IEEE Access 8 (2020) 130551–130560.
[10] Y. Iwata, H.T. Thanh, G. Sun, K. Ishibashi, High accuracy heartbeat detection from CW-Doppler radar using singular value decomposition and matched filter, Sensors 21 (11) (2021) 3588.
[11] L. Antognoli, S. Moccia, L. Migliorelli, S. Casaccia, L. Scalise, E. Frontoni, Heartbeat detection by laser Doppler vibrometry and machine learning, Sensors 20 (18) (2020) 5362.
[12] M. Ali, A. Elsayed, A. Mendez, Y. Savaria, M. Sawan, Contact and remote breathing rate monitoring techniques: a review, IEEE Sens J 21 (13) (2021) 14569–14586.
[13] X. Qiao, G. Li, T. Shan, R. Tao, Human activity classification based on moving orientation determining using multistatic micro-Doppler radar signals, IEEE Trans. Geosci. Rem. Sens. 60 (2021) 1–15.
[14] H. Xu, M.P. Ebrahim, K. Hasan, F. Heydari, P. Howley, M.R. Yuce, Accurate heart rate and respiration rate detection based on a higher-order harmonics peak selection method using radar non-contact sensors, Sensors 22 (1) (2021) 83.
[15] T. Kitagawa, K. Yamamoto, T. Ohtsuki, Non-contact heartbeat detection based on beam diversity using multibeam Doppler sensor, in: 2021 IEEE Global Communications Conference (GLOBECOM), IEEE, 2021, pp. 1–6.
[16] K. Yamamoto, T. Ohtsuki, Non-contact heartbeat detection by heartbeat signal reconstruction based on spectrogram analysis with convolutional LSTM, IEEE Access 8 (2020) 123603–123613.
[17] J. Saluja, J. Casanova, J. Lin, A supervised machine learning algorithm for heart-rate detection using Doppler motion-sensing radar, IEEE J Electromagn RF Microw Med Biol 4 (1) (2020) 45–51, https://doi.org/10.1109/JERM.2019.2923673.
[18] V.L. Petrović, M.M. Janković, A. V Lupšić, V.R. Mihajlović, J.S. Popović-Božović, High-accuracy real-time monitoring of heart rate variability using 24 GHz continuous-wave Doppler radar, IEEE Access 7 (2019) 74721–74733, https://doi.org/10.1109/ACCESS.2019.2921240.
[19] Z.-K. Yang, S. Zhao, X.-D. Huang, W. Lu, Accurate Doppler radar-based heart rate measurement using matched filter, IEICE Electron. Express 17 (8) (2020) 20200062, https://doi.org/10.1587/elex.17.20200062.
[20] S. Izumi, T. Okano, D. Matsunaga, H. Kawaguchi, M. Yoshimoto, Non-contact instantaneous heart rate extraction system using 24-GHz microwave Doppler sensor, IEICE Trans. Commun. E102.B (6) (2019) 1088–1096, https://doi.org/10.1587/transcom.2018HMP0007.
[21] Q. Lv, et al., Doppler vital signs detection in the presence of large-scale random body movements, IEEE Trans Microw Theory Tech 66 (9) (2018) 4261–4270, https://doi.org/10.1109/TMTT.2018.2852625.
[22] A. Nocera, et al., Machine Learning in RADAR-Based Physiological Signals Sensing: A Scoping Review of the Models, Datasets and Metrics, 2021.
[23] R. Bagwe, J. Kachhia, A. Erdogan, K. George, Automated radar signal analysis based on DL, in: 2020 10th Annual Computing and Communication Workshop and Conference, CCWC 2020, Institute of Electrical and Electronics Engineers Inc., Jan. 2020, pp. 215–221, https://doi.org/10.1109/CCWC47524.2020.9031240.
[24] K. Chen, Y. Duan, Y. Huang, W. Hu, Y. Xie, A DL method of human identification from radar signal for daily sleep health monitoring, Bioengineering 11 (1) (Jan. 2024), https://doi.org/10.3390/bioengineering11010002.
[25] S. Śmigiel, K. Pałczyński, D. Ledziński, DL techniques in the classification of ecg signals using r-peak detection based on the ptb-xl dataset, Sensors 21 (24) (Dec. 2021), https://doi.org/10.3390/s21248174.
[26] Y. Xiang, J. Guo, M. Chen, Z. Wang, C. Han, MAE-based self-supervised pretraining algorithm for heart rate estimation of radar signals, Sensors 23 (18) (Sep. 2023), https://doi.org/10.3390/s23187869.
[27] J.H. Choi, J.E. Kim, K.T. Kim, DL approach for radar-based people counting, IEEE Internet Things J. 9 (10) (May 2022) 7715–7730, https://doi.org/10.1109/JIOT.2021.3113671.
[28] D. Toda, R. Anzai, K. Ichige, R. Saito, D. Ueki, ECG signal reconstruction using FMCW radar and a convolutional neural network for contactless vital-sign sensing, IEICE Trans. Commun. E106B (1) (Jan. 2023) 65–73, https://doi.org/10.1587/transcom.2022EBP3005.
[29] S. Siuly, S.K. Khare, E. Kabir, M.T. Sadiq, H. Wang, An efficient Parkinson's disease detection framework: leveraging time-frequency representation and AlexNet convolutional neural network, Comput. Biol. Med. 174 (2024) 108462.
[30] L. Zheng, et al., AnnoPRO: a strategy for protein function annotation based on multi-scale protein representation and a hybrid DL of dual-path encoding, Genome Biol. 25 (1) (2024) 41.
[31] M. Mou, et al., A transformer-based ensemble framework for the prediction of protein–protein interaction sites, Research 6 (Apr. 2024) 240, https://doi.org/10.34133/research.0240.
[32] Y. Wang, et al., A task-specific encoding algorithm for RNAs and RNA-associated interactions based on convolutional autoencoder, Nucleic Acids Res. 51 (21) (2023) e110, e110.
[33] S. Schellenberger, et al., A dataset of clinically recorded radar vital signs with synchronised reference sensor signals, Sci. Data 7 (1) (2020) 291.
[34] T.-Y. Lin, P. Dollár, R. Girshick, K. He, B. Hariharan, S. Belongie, Feature pyramid networks for object detection, in: Proceedings of the IEEE Conference on Computer Vision and Pattern Recognition, 2017, pp. 2117–2125.
[35] Z. Zhuang, et al., Nipple segmentation and localization using modified U-net on breast ultrasound images, J. Medical Imaging Health Informatics 9 (2019) 1827–1837.
[36] A. Chaurasia, E. Culurciello, Linknet: exploiting encoder representations for efficient semantic segmentation, in: 2017 IEEE Visual Communications and Image Processing (VCIP), IEEE, 2017, pp. 1–4.
[37] F. Michler, et al., A clinically evaluated interferometric continuous-wave radar system for the contactless measurement of human vital parameters, Sensors 19 (11) (2019) 2492.
[38] C. Will, et al., Radar-based heart sound detection, Sci. Rep. 8 (1) (2018) 11551.
[39] J. Chen, D. Zhang, Z. Wu, F. Zhou, Q. Sun, Y. Chen, Contactless ECG monitoring with millimeter wave radar, IEEE Trans Mob Comput (2022).
[40] Z. Xia, M.M.H. Shandhi, O.T. Inan, Y. Zhang, Non-contact sensing of seismocardiogram signals using microwave Doppler radar, IEEE Sens J 18 (14) (2018) 5956–5964.
[41] Y. Ran, D. Zhang, J. Chen, Y. Hu, Y. Chen, Contactless blood pressure monitoring with mmWave radar, in: GLOBECOM 2022-2022 IEEE Global Communications Conference, IEEE, 2022, pp. 541–546.
[42] S. Mahmud, et al., NABNet: a nested attention-guided BiConvLSTM network for a robust prediction of blood pressure components from reconstructed arterial blood pressure waveforms using PPG and ECG signals, Biomed. Signal Process Control 79 (2023) 104247.
[43] N. Ibtehaz, et al., PPG2ABP: translating photoplethysmogram (PPG) signals to arterial blood pressure (ABP) waveforms, Bioengineering 9 (11) (2022) 692.
[44] A. Rahman, et al., Fetal ECG extraction from maternal ECG using deeply supervised LinkNet++ model, Eng. Appl. Artif. Intell. 123 (2023) 106414.
[45] S. Mahmud, M.S. Hossain, M.E.H. Chowdhury, M.B.I. Reaz, MLMRS-Net: electroencephalography (EEG) motion artifacts removal using a multi-layer multi-resolution spatially pooled 1D signal reconstruction network, Neural Comput. Appl. 35 (11) (2023) 8371–8388.
[46] M.S. Hossain, et al., MultiResUNet3+: a full-scale connected multi-residual UNet model to denoise electrooculogram and electromyogram artifacts from corrupted electroencephalogram signals, Bioengineering 10 (5) (2023) 579.
[47] J.E. Hall, Pocket Companion to Guyton & Hall Textbook of Medical Physiology E-Book, Elsevier Health Sciences, 2015.
[48] L. Pstras, K. Thomaseth, J. Waniewski, I. Balzani, F. Bellavere, The Valsalva manoeuvre: physiology and clinical examples, Acta Physiol. 217 (2) (2016) 103–119.
[49] J.V. Rundo, Obstructive sleep apnea basics, Cleve. Clin. J. Med. 86 (9 Suppl 1) (2019) 2–9.
[50] L. Yaroslavsky, How to Optimally Sample and Resample Images: Theory and Methods Using MATLAB, vol. 3, Bentham Science Publishers, 2020.
[51] H. Meng, Y.L. Guan, S. Chen, Modeling and analysis of noise effects on broadband power-line communications, IEEE Trans. Power Deliv. 20 (2) (2005) 630–637.
[52] M.S. Hossain, et al., Motion artifacts correction from EEG and fNIRS signals using novel multiresolution analysis, IEEE Access 10 (2022) 29760–29777.
[53] M.S. Hossain, et al., Motion artifacts correction from single-channel EEG and fNIRS signals using novel wavelet packet decomposition in combination with canonical correlation analysis, Sensors 22 (9) (2022) 3169.
[54] S. Mahmud, et al., A shallow U-Net architecture for reliably predicting blood pressure (BP) from photoplethysmogram (PPG) and ECG (ECG) signals, Sensors 22 (3) (2022) 919.
[55] R. Takahashi, T. Matsubara, K. Uehara, Data augmentation using random image cropping and patching for deep CNNs, IEEE Trans. Circ. Syst. Video Technol. 30 (9) (2019) 2917–2931.
[56] N. Ibtehaz, M.S. Rahman, MultiResUNet: rethinking the U-Net architecture for multimodal biomedical image segmentation, Neural Network. 121 (2020) 74–87.
[57] R.N. Youngworth, B.B. Gallagher, B.L. Stamper, An overview of power spectral density (PSD) calculations, Optical manufacturing and testing VI 5869 (2005) 206–216.
[58] Y. Mu, X. Liu, L. Wang, A Pearson's correlation coefficient based decision tree and its parallel implementation, Inf. Sci. 435 (2018) 40–58.
[59] H. Zhang, M. Zhao, C. Wei, D. Mantini, Z. Li, Q. Liu, EEGdenoiseNet: a benchmark dataset for DL solutions of EEG denoising, J. Neural. Eng. 18 (5) (2021) 056057.